Biointerface Research in Applied Chemistry
Open-Access Journal (ISSN: 2069-5837)

Article
Volume 13, Issue 3, 2023, 255
https://doi.org/10.33263/BRIAC133.255

Cisplatin Encapsulation Efficiency Profiles using Titania Nanotube Arrays Platform in Targeted Cancer Therapy

Wan Nuramiera Faznie Wan Eddis Effendy [1], Rabiatul Basria S. M. N. Mydin [1,*], Srimala Sreekantan [2], Amirah Mohd Gazzali [3], Muhammad Yusri Musa [4]

[1] Department of Biomedical Science, Advanced Medical and Dental Institute, Universiti Sains Malaysia, 13200 Kepala Batas, Pulau Pinang, Malaysia; rabiatulbasria@usm.my (R.B.S.M.N.M); amierafaznie@gmail.com (W.N.F.W.E.E);
[2] School of Materials and Mineral Resources Engineering, Universiti Sains Malaysia, Engineering Campus, 14300, Nibong Tebal, Pulau Pinang, Malaysia; srimala@usm.my (S.S);
[3] School of Pharmaceutical Sciences, Universiti Sains Malaysia, 11800, Minden, Pulau Pinang, Malaysia; amirahmg@usm.my (A.M.G);
[4] Department of Clinical Medicine, Advanced Medical and Dental Institute, Universiti Sains Malaysia, 13200 Kepala Batas, Pulau Pinang, Malaysia; myusrim@usm.my (M.Y.M.)
* Correspondence: rabiatulbasria@usm.my (R.B.S.M.N.M);

Scopus Author ID 5652142500
Received: 14.03.2022; Accepted: 16.05.2022; Published: 10.06.2022

Abstract: Titania nanotube arrays (TNA) nanosystem has been discussed widely in drug delivery applications that could provide advantages for sustaining chemo drug release in targeted cancer therapy. This study profiled the cisplatin chemo drug (CDDP) encapsulation efficiency on TNA (CDDP–TNA). Anatase TNA nanosystem used in this study present with diffraction angle 25 θ and 48 θ. The distribution and binding interaction of CDDP on TNA were identified using the primary functional marker amide I band (N–H), and the sustained release profile of CDDP from TNA was further captured. Furthermore, CDDP–TNA nanosystem is present with favorable hydrophilic properties that could facilitate the effective release of CDDP from TNA nanosystem. However, developing a controlled release model of CDDP -TNA nanosystem using polymer coating technology is needed to support the present finding, especially in targeted cancer therapy applications.

Keywords: cisplatin; drug delivery nanosystem; encapsulation efficiency; targeted cancer therapy; titania nanotube arrays.

1. Introduction

The potential of titania nanotube arrays (TNA) in drug delivery has already been acknowledged in countless studies [1, 2]. Compared to other forms of titanium dioxide, TNA was preferable for drug delivery due to its nanotube structure, which generally has a larger surface area per volume and is hydrophilic [3]. Chemodrugs have also been investigated for drug loading into TNA for cancer therapy and anti-inflammatory agents, vitamins, and genes [4], demonstrating their prospect in drug delivery. These properties supported the study of drug-loaded TNA in sustaining and prolonging release activity over the study period. Some hydrophilic chemodrugs, such as CDDP and doxorubicin [4], are also studied together with TNA for controlled drug release activity. These drugs are easier to incorporate through passive diffusion into body fluid than hydrophobic ones [5]. Additionally, the one-open-ended nanotube structure of TNA increases drug loading efficiency and slowers drug release in the

presence or absence of a polymer, thus minimizing drug burst release. Eventually, using TNA may prevent and reduce the toxicity induced by exposure to high doses of chemodrugs.

Chemodrug cisplatin (CDDP) was the standard gold treatment for various cancers such as cervical, breast, nasopharyngeal, colon, and neuroblastoma [6]. Aldossary [7] reported that the mechanism of action of CDDP is associated with the potential of CDDP to cross-link with the uracil bases on DNA to produce DNA adducts that cause DNA damage and induce cancer cell death by blocking DNA repair. However, several limitations have been recognized since CDDP was being applied in cancer therapy, such as developing resistant cancer cells, hypersensitivity, and organ failure due to continuous exposure. Sobczak [8] reported that the use of CDDP for cancer treatment had achieved its limits, given that a single treatment with CDDP is ineffective, as seen in non-small lung cancer. Localized and targeted therapy, which aims to increase the effectiveness of chemo drug treatment at the level of proteins or genes highly associated with cancer development while avoiding non-specific drug binding, has been introduced by Song *et al*. [9], which TNA as nanocarrier as presented in work by Effendy *et al*. [10]. The potential of CDDP-loaded TNA had shown a positive outcome on nasopharyngeal carcinoma; however, the method and encapsulation efficiency had not been properly addressed. The present work was performed to address the procedure of CDDP loading and maintain the effectiveness of CDDP against cancer cells. The optimal morphological parameters of TNA for CDDP loading were discussed throughout the study, especially on the characterization profiles.

2. Materials and Methods

2.1. Study samples.

The TNA nanosystem was fabricated by electrochemical anodization where ion exchange between fluoride salt and the titanium surface takes place following protocol by Effendy *et al*. [11]. Cisplatin (CDDP) (Platol^{TM}) was obtained from Venus Remedies Limited, India. The handling procedure was carried out under the supervision of the Department of Pharmacy HUSM@Bertam, Advanced Medical and Dental Institute, Universiti Sains Malaysia. The sample size of TNA was measured at 1 x 1 cm; meanwhile, the concentration of CDDP used was 1 mg/mL throughout the study.

2.2. Optimization of CDDP loading on TNA.

The method of CDDP-TNA was determined between immersion [12] and the top-filling method from a study by Shirazi-Fard *et al*. [13]. Through immersion, the TNA was placed individually containing 300 µL of CDDP and allowed to be incubated for 24 h at 4 ºC. on the other hand, top-filling was performed by pipetting 50 µL of CDDP on top of each TNA side. Next, all samples were dried in several methods, such as air-drying under airflow of a biosafety cabinet (BSC) which was approximately 120 mins, and vacuum dried (90 mins).

2.3. Encapsulation efficiency profiles of CDDP-TNA.

Encapsulation efficiency of the CDDP-TNA was determined by the weight differences between TNA and CDDP-TNA as stated in equation 1.1 as adapted from Hamedi & Koosha [14]. On the other hand, the encapsulation efficiency was spectrophotometrically measured at a wavelength of 706 nm according to Zakeri *et al*. [15] by using PowerWave^{TM} BioTek, USA,

where calculation stated in equation 1.2. The CDDP was loaded on both sides of TNA surfaces for the weight difference, and the weight was recorded. The process was repeated five times, with weight recorded for each loading process. Next, for absorbance measurement, the CDDP-TNA (one-time loading) was immersed in 2 mL phosphate buffer saline (PBS) and subsequently sonicated in a water bath at 37 ºC for 30 mins. The absorbance reading of CDDP was performed according to Basotra *et al.* [16]. Briefly, the 100 µL immersed PBS was withdrawn and mixed with o-phenylenediamine (OPDA). Next, the mixture was heated at 100 ºC for 10 mins before being cooled down at room temperature (RT). The procedure resulted in the formation of a green complex which dissolved with the addition of dimethylformamide (DMF) and phosphate buffer at pH 6.8, which is illustrated in Figure 1. The sample was properly mixed and submitted for absorbance reading at 706 nm. The loading efficiency was calculated according to equation 1.2.

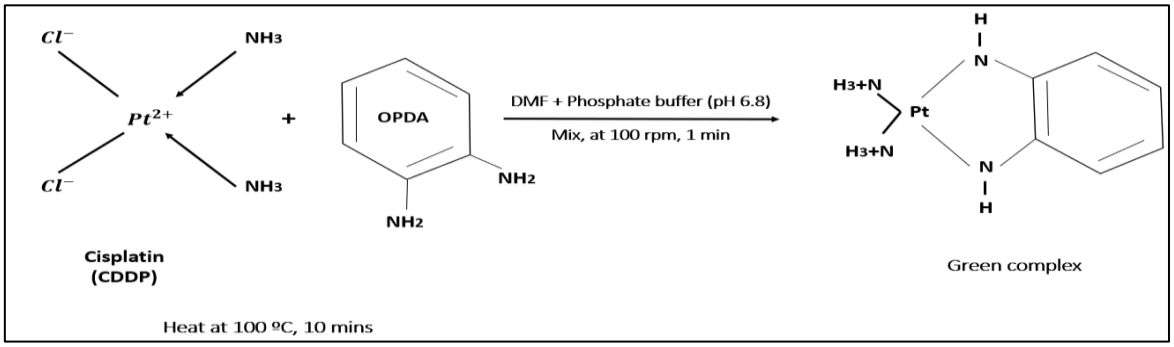

Figure 1. Flowchart of CDDP detection. An illustrative graphic of CDDP detection was adapted from Fisher *et al.* [17]. The CDDP concentration was determined by a method adapted from Basotra *et al.* [16] in CDDP, OPDA, phosphate buffer pH 6.8, and DMF with ratio (1:1:2:6).

Equation 1.1 Loading efficiency (%)

$$= \frac{Weight\ after\ loading - Initial\ weight}{Initial\ weight} x\ 100$$

Equation 1.2 Encapsulation efficiency (%)

$$= \frac{Absorbance\ of\ CDDP\ solution - Absorbance\ of\ PBS}{Absorbance\ of\ CDDP\ (100\%)}\ x\ 100$$

2.4. Characterisations of CDDP-TNA nanosystem.

The anodized sample was subjected for XRD analysis using a diffractometer (Philips PW1729 powder X, Bruker D8) with brookite (1 2 1) at 2θ = 30 °, rutile (1 1 0) at (2θ = 28 °) and anatase (1 0 1) 2θ = 25 ° according to Patil *et al.* [18]. FTIR spectroscopy Frontier NIR Spectrometer, L1280026 Perkin Elmer (USA) analysis was performed between 4000 – 500 cm^{-1} to confirm the presence of chemical interactions between TNA, CDDP-TNA, and after chitosan coating. The result was analyzed by Spectrum (PerkinElmer, USA) software to determine the functional groups present in the spectrum obtained.

2.5. Water contact angle measurement.

Formation of water contact angle due to interaction of the solid-liquid, liquid surface tension, and free surface energy of solid sample was observed in wettability analysis. Observation and measurement of water contact of TNA nanosystem, CDDP-TNA, chitosan-coated CDDP-TNA, and post-release samples were carried out after the sample was wholly

dried under BSC airflow. A total of 20 µL of sterile deionized water was dropped on top of the TNA nanosystem, and five angles of wettability were captured and measured using a goniometer (Rame-Hart 260, DROPimage Advanced V2.5). The results were statistically analyzed by paired t-test and presented as mean ± SD for each sample.

3. Results and Discussion

3.1. Crystallinity phase of TNA.

The XRD profiles of Ti and the un-annealed and annealed TNA nanosystem are presented in Figure 2. The results indicated that the anatase crystal size of the un-annealed nanosystem was smaller than that of the annealed TNA nanosystem. At the same position, the crystallite size of the annealed TNA nanosystem (35.55 ± 3.91 nm) had slightly increased compared with that of the un-annealed TNA nanosystem (35.00 ± 5.01 nm). The two new peaks (red ring) at positions 25 θ and 48 θ indicated the crystalline properties of the TNA nanosystem compared to un-annealed TNA. Both had a crystallite size of approximately 20 - 26 nm. These two peaks indicated the anatase crystalline phase of TNA. The sharp peaks of 25 θ at 35 θ, 38 θ, 40 θ, and 70 θ indicated the presence of the anatase structure from the anodization and annealing of the TNA nanosystem, indicating that TNA was grown in a stable manner using an electrochemical anodization method on Ti foil in an organic electrolyte. The anatase phase of TNA has been chosen in many studies for drug delivery applications because it attracts cells and promotes drug-TNA interaction [19].

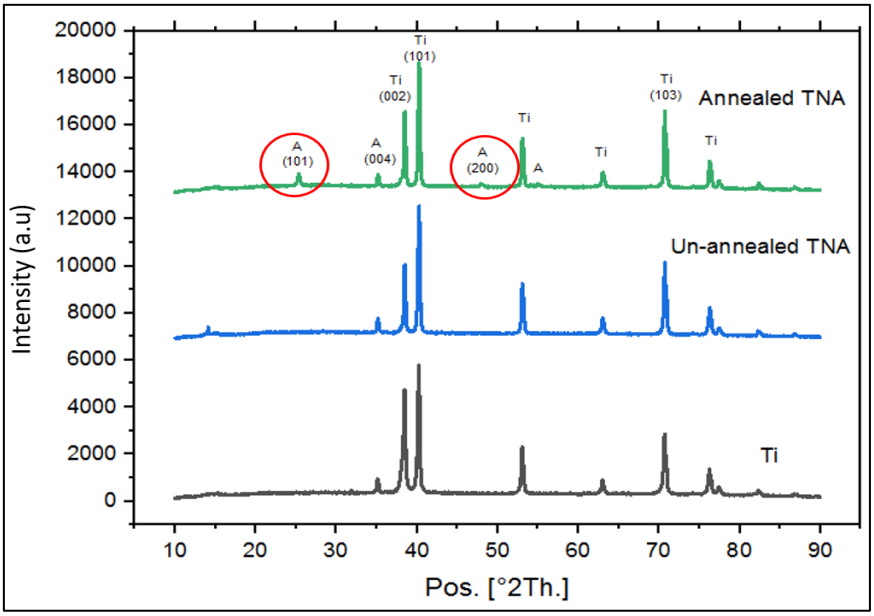

Figure 2. XRD analysis of Ti, the un-annealed TNA nanosystem, and the annealed TNA system. The formation of new peaks is labeled with a red arrow to indicate the changes in the crystallinity phase. The Ti peak represented the substrate, whereas the anatase (A) represented the TNA nanosystem's crystallinity shape.

The surface crystallinity of the TNA nanosystem surface plays an essential role in cell adhesion and stability of biomedical implants [20, 21]. The electrostatic feature of the anatase TNA nanosystems favors cell attachment in the presence of Ti-OH groups [22]. Moreover, Keeley and co-workers [23] described that the anatase phase of the Ti surface could promote the antibacterial characteristic compared with the un-annealed samples. Therefore, the end-product of TNA nanosystem EA was ensured in the anatase phase by heat treatment at 400 ºC

as performed by Hazan *et al*. [24]. In addition, anatase phase TNA was preferable for apatite formation to amorphous [25], which is important in promoting slower drug release. Moreover, the anatase phase of the TNA nanosystems in biomedical implant study promoted stability, creating a desirable surface for cell attachment and platelet activation for further work.

3.2. The weight difference of CDDP-TNA.

The mean difference from the initial weight after five loading cycles was 2.81 ± 1.09 %, and that after one loading cycle was 0.18 ± 1.96 %, as tabulated in Table 1. This study found that loading efficiency was not finalized by weight difference. The t-test found no significant difference between the number of CDDP loading cycles and CDDP-TNA weight with the non-CDDP-loaded TNA nanosystem reference ($p > 0.05$).

Table 1. The weight difference of TNA before and after CDDP loading. The data were collected in two independent experiments.

Number of loading (s)	**1x**	**2x**	**3x**	**4x**	**5x**
Final weight after CDDP loading	57.1 ± 1.12	58.0 ± 1.02	58.2 ± 1.41	58.4 ± 0.94	58.6 ± 0.62
Mean weight difference (%)	0.18 ± 1.96	1.75 ± 1.79	2.11 ± 2.47	2.46 ± 1.65	2.81 ± 1.09

Initial weight: 57.0 ± 0.93 mg, n = 5.

Two methods of CDDP loading and encapsulation efficiency were studied; the weight difference before and after CDDP loading and absorbance upon post-release from the standard curve (Table 2). Loading and encapsulation efficiency was calculated based on Pharmacopeia of the People's Republic of China [26]. Drug loading efficiency was measured based on the weight difference of materials before and after drug loading in percentage according to Husain *et al*. [27], as presented in Table 1. The weight of the TNA nanosystem upon addition of CDDP was varied and showed no constant pattern even though two independent replicates were measured. In this work, the loading efficiency depending on weight was excluded, whereas spectrophotometer measurement was used as the sole method for CDDP quantification. CDDP was measured by calculating the cumulative release over time with the standard curve of CDDP (data was excluded).

The CDDP loading method was determined by testing several standard procedures as tabulated in Table 2. The CDDP loading method played an essential role in the nano delivery system, which ensured the success of the therapy. Two ways of CDDP loading were applied: top-filling [28] and immersion methods, referred to and modified accordingly [29, 30]. Compared to Wong and Duduo's [31] works, the practice of the incubation temperature and drying method was different. After reconstitution, the immersion method was conducted at a low temperature to maintain the CDDP properties, as referred to Al-Zomor *et al*. [32]. All procedures were carried out in minimal light at RT to maintain the stability of CDDP in 0.9 % [v/v] sodium chloride. In addition, the aliquot CDDP was kept at -4 ºC (for the short term) and -20 ºC (long term) upon enclosing the vial, according to Shaaban *et al*. [33].

3.3. CDPP-TNA loading efficiency on different lengths of TNA.

TNA nanosystems were prepared with a standardized voltage of 30 V with various anodization periods; CDDP-TNA nanosystem drying techniques and CDDP loading methods are tabulated in Table 2. The samples anodized at 30 mins were denoted as A, while samples

anodized at 60 mins were denoted as B. A1–A4 recorded loading efficiencies of 47.94 ± 0.33 %, 3.12 ± 0.05 %, 55.74 ± 0.41 %, and 0.78 ± 0.14 %, respectively.

Table 2. CDDP loading efficiency onto TNA nanosystem with different nanotube lengths via different loading methods. CDDP-TNA loaded via the top-filling method on samples anodized at 60 mins recorded the highest efficiency of 98.95 ± 7.02 %. The vacuum-drying technique exhibited the next-highest efficiency.

Samples	Anodization period (mins)	Vacuum		Method of loading	Loading efficiency (%)
		Yes	No		
A1	30	/		Top filling	47.94 ± 0.33
A2		/		Immersion	3.12 ± 0.05
A3			/	Top filling	55.74 ± 0.41
A4			/	Immersion	0.78 ± 0.14
B1	60	/		Top filling	98.95 ± 7.02
B2		/		Immersion	11.57 ± 0.23
B3			/	Top filling	97.69 ± 0.62
B4			/	Immersion	12.42 ± 0.36

Compared with A, B1–B4 displayed higher efficiencies of 98.95 ± 7.02 %, 11.57 ± 0.23 %, 97.69 ± 0.62 % and 12.42 ± 0.36 %, respectively. Comparing TNA nanosystem lengths and drying techniques revealed that the long TNA nanosystem (B) demonstrated high CDDP uptake with amounts ranging from 11.57 ± 0.23 % to 98.95 ± 7.02 % regardless of CDDP loading methods and drying techniques. By contrast, A showed a CDDP uptake rate of approximately 0.78 ± 0.14 % to 47.94 ± 0.33 %. CDDP has detected an approximately 8.5-fold increase in CDPP-TNA, which was prepared by subjecting the TNA nanosystem to immersion and top-filling at 800 nm (60 mins). CDDP took 90 minutes to dry under vacuum drying but took approximately 120 mins to dry under BSC.

Significant differences between groups were analysed and displayed in Figure 3. The TNA nanosystem prepared through different CDDP loading methods and anodised at 60 mins showed significant differences regardless of the sample drying techniques used.

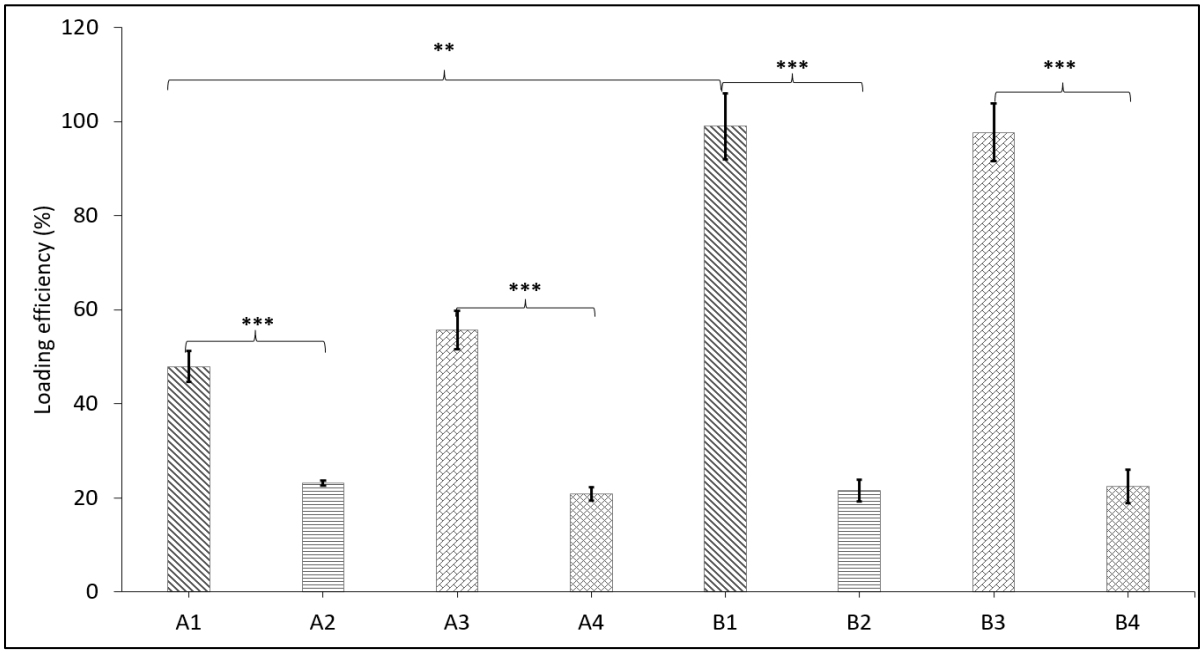

Figure 3. Histogram displaying the loading efficiency of the TNA nanosystem under various CDDP loading conditions. Vacuum drying showed a more significant difference (**) than the nonvacuum sample, whereas the top-filling method displayed higher efficiency (**) than the overnight immersion. Compared with the TNA nanosystem anodized for 30 mins at 300 nm, the TNA nanosystem anodized for 60 mins at 800 nm demonstrated longer lengths and higher CDDP encapsulation efficiency. $p < 0.05$ (*) and $p < 0.01$ (**), $n = 3$.

Significant differences were found for A1–A2 and A3–A4 ($p = 0.000$), as well as for A2–A4 ($p = 0.023$). Significant differences were also demonstrated by B1–B2 ($p = 0.000$), B2–B4 ($p = 0.042$) and B3–B4 ($p = 0.000$). No significant difference was observed for A1–A3 ($p = 0.191$), B1–B3 ($p = 0.812$), A2–B2 ($p = 0.215$) and A3–B3 ($p = 0.317$). The results for between-group comparison were as follows: A1–B1 ($p = 0.011$) and A4–B4 ($p = 0.032$).

3.4. Characterisations of CDDP-TNA.

3.4.1. FTIR analysis.

The FTIR profiles of the TNA, CDDP-TNA, and chitosan-coated TNA nanosystems are tabulated in Table 3 and displayed in Figure 4. The FTIR spectrum of TNA was screened at 2176 and 595 cm^{-1}.

Table 3. FTIR peak assignments for TNA nanosystem. The major peaks for CDDP and chitosan are hydroxyl, amide I, and amine.

Peak assignment	Value (cm^{-1})
Ti-O-Ti	595
C-N (amine)	1029
O-H (hydroxyl)	1412
N-O (nitro)	1544
Ti-OH/ N-H (amide I)	1638
CH_2	2163
O-H / N-H	3376

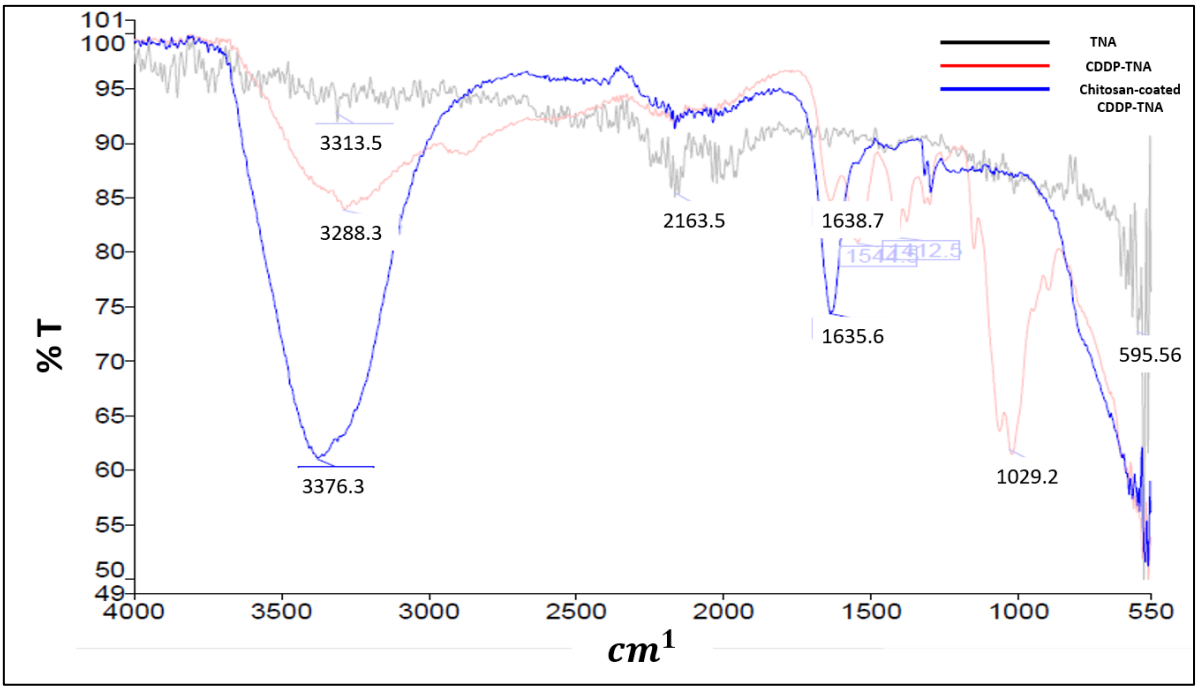

Figure 4. FTIR analysis of TNA, CDDP-TNA, and chitosan-coated CDDP-TNA. The peaks at 2176 and 595 cm^{-1} indicated TNA's Ti–O–Ti stretching band peaks. The presence of CDDP was identified based on the peak in the FTIR spectrum at 1671 cm^{-1}.

The presence of TNA nanosystem peaks was constant for all the samples demonstrating the unchanged form of the TNA during the study period. In particular, the stretching of Ti–O–Ti bands from the TNA nanosystem structure was noted. The peak at 2176 cm^{-1} disappeared after CDDP loading and chitosan coating, as shown in Figure 4. FTIR spectrum of CDDP-TNA

that falls on 3369 cm^{-1} suggests the presence of O–H bands. Two possible bands at 1299 cm^{-1} were observed and were attributed to the twisting of CH_2 or C–O–C bands that could be ascribed to the introduction of CDDP via the top-filling method. Critical spectrum detection indicated the presence of CDDP at 1643 cm^{-1} and pointed out the presence of amide I (N–H) in the CDDP structure. This result demonstrated that CDDP had been successfully loaded and conjugated onto the TNA nanosystem.

The extended bands of the O–H groups were seen at approximately 3316 cm^{-1} CH_2 bands stretching at 1546 cm^{-1}, C–H bands at 1412 cm^{-1}, and C–O–C band stretching (1030 cm^{-1}) were observed. These results indicated that the chitosan coating was present on the CDDP-TNA nanosystem. The disappearance of the peak at 1643 cm^{-1} indicated that chitosan had been thoroughly coated. Several types of C–H bands, which were determined based on chitosan, were seen in the spectrum of the chitosan-coated CDDP-TNA sample related to the chitosan structure, which is made up of polysaccharides. The top-filling method resulted in the appropriate incorporation of chitosan onto the CDDP-TNA surface as supported by C, which is the main component of chitosan.

3.5. Wettability analysis of CDDP-TNA.

The TNA nanosystems showed contact angles ranging from 37.24 ± 0.16 ° to 70.04 ± 0.63 °. This result suggested that the TNA nanosystems are hydrophilic, given that the angles were less than 90 °, as demonstrated in Figure 5. The wettability angle increased to 43.57 ± 0.03 ° after CDDP addition to the TNA nanosystem because CDDP also presented hydrophilic properties. After adding chitosan, the wettability of the TNA nanosystem increased, as noted by the increment in wettability angle to 70.04 ± 0.63 °. The surface wettability of Ti and TNA showed a significant difference ($p = 0.000$). This outcome of Ti anodization made the surface hydrophilic, which is essential in implantation. On the other hand, CDDP, which possessed hydrophilic properties, had not statistically changed the wettability of the TNA ($p = 0.382$). Next, chitosan coating had a significant effect compared to TNA and CDDP-TNA with $p = 0.000$. Moreover, the statistical analysis of TNA wettability and chitosan-coated CDDP-TNA also presented significant differences ($p = 0.001$).

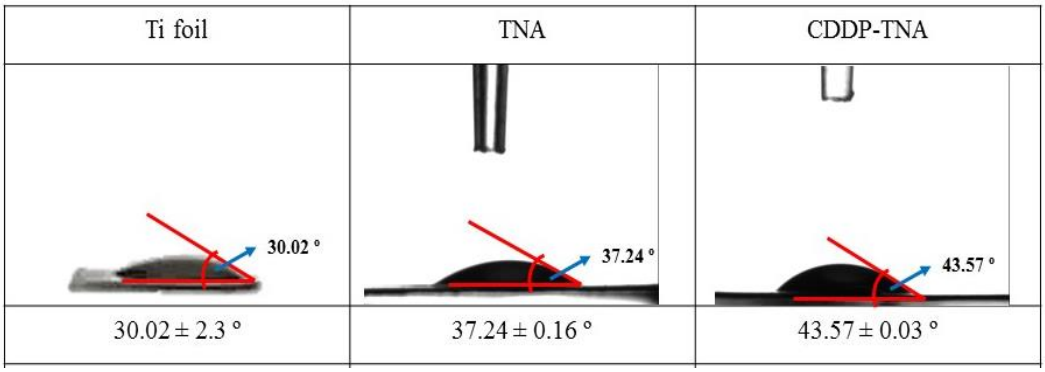

Figure 5. Wettability analysis of the studied sample. The water contact angle of each sample was examined by using a goniometer and visualized using ImageJ software. The angle of wettability was displayed as mean ± SD (n = 5).

Hydrophobicity or hydrophilicity properties of a material are among the most critical parameters affecting the biological response to an implanted biomaterial and profoundly influencing the cell behavior during osseointegration, which begins when the implant comes into contact with the blood [34]. Chitosan-coated CDDP-TNA presented with high

hydrophilicity, as seen in Figure 5. The wettability increased with the addition of the CDDP and chitosan coating, which was conducive to implantation. Wettability affects platelet adhesion or activation, blood coagulation, cell and bacterial adhesion, and protein adsorption [35]. Highly hydrophilic surfaces are more preferred than hydrophobic ones, given their desirable interactions with biological fluids, cells, and tissues. The adsorption behavior and protein adhesion on the implant surface depends on the surface properties. Therefore, a decrease in these parameters increases the surface wettability capacity [36]. This work had successfully developed a water-soluble chitosan-coated CDDP-TNA nanosystem, including the foremost importance in the CDDP release profile and further discussion of the *in vitro* interaction.

The potential of the TNA nanosystem in CDDP loading and delivery has been comprehensively studied, focusing on the morphology of the TNA nanosystem and the method of CDDP loading. The optimum parameters of the TNA nanosystem for CDDP delivery are presented in Table 2. The surface morphology of the TNA nanosystem morphology of more than 30 nm was agreed well with the exploration of drug release [37], which supported our work on growing the TNA nanosystem with an inner diameter of 60 nm. Wang *et al*. [38] mentioned that the best range of TNA's diameter appeared to be 15-100 nm, which fitted the design of the TNA nanosystem. In addition, the parameters of the TNA nanosystem were depicted for cell attachment and proliferation, especially for biomedical implantation.

The encapsulation efficiency of the drug was influenced by the length of the TNA nanosystem in which the longer the nanotube, the more drug can be loaded; thus, more extended release can be achieved [39]. This work presented with more than 95 % loading efficiency at approximately 800 nm length. In general, when longer nanotubes are used in drug loading, more drugs will be entrapped on the wall and surface of the open-ended TNA nanosystem, causing a slow drug release rate. However, Jafari *et al*. [40] described that those nanotubes longer than 1 μm cause interfacial stress and nanotube breakdown when applied for implantation, resulting in the design of a TNA nanosystem with less than 1 μm length for this present work. Aside from length, the diameter of the TNA appeared to have an impact on drug loading and release, with the optimum parameter being in the range of 30 to 80 nm [41], which was retained in each anodization cycle of our study. The applied diameter, on the other hand, was significantly dependent on the sample target, which may be bacteria or cell lines. Encapsulation efficiency of drugs loaded into TNA nanosystems will be a key factor in determining the efficacy of drug delivery using TNA nanosystems as nanocarriers in the future, particularly for cancer therapy.

4. Conclusions

In this work, the hydrophilic properties of the TNA play a vital role in CDDP loading and the loading method by top filling vacuum technique. The interaction of CDDP with TNA was described in detail, especially on the nanocomplex surface properties that could promote the highest encapsulation efficiency. Further characterization of the CDDP stability in the TNA nanosystem, including controlled release potential using biopolymer coating approaches, is needed, especially in understanding the potential of this nanosystem in targeted cancer therapy applications.

Funding

This research was funded by Universiti Sains Malaysia, RUI EKSESAIS 2019 (No:1001/CIPPT/8012338).

Acknowledgments

We would also like to express gratitude to the staff from the School of Materials and Mineral Resources Engineering and Centre for Global Archaeological Research, Universiti Sains Malaysia, for their assistance with characterization tests.

Conflicts of Interest

The authors declare no conflict of interest.

References

1. Xu, Y.; Zhao, C.; Zhang, X.; Xu, J.; Yang, L.; Zhang, Z.; Gao, Z.; Song, Y.Y. Engineering tailorable TiO_2 nanotubes for NIR-controlled drug delivery. *Nano Res.* **2021**, *14*, 4046-4055, https://doi.org/10.1007/s12274-021-3338-7.
2. Park, J.; Cimpean, A.; Tesler, A.B.; Mazare, A. Anodic TiO_2 Nanotubes: Tailoring Osteoinduction via Drug Delivery. *Nanomaterials* **2021**, *11*, 2359, https://doi.org/10.3390/nano11092359.
3. Lin, Y.; Zhang, L.; Yang, Y. *et al*. Loading Gentamicin and Zn^{2+} on TiO_2 Nanotubes to Improve Anticoagulation, Endothelial Cell Growth, and Antibacterial Activities. *Stem Cells Int*. **2021**, *2021*, https://doi.org/10.1155/2021/9993247.
4. Ashrafizadeh, M.; Mirzaei, S.; Gholami, M.H. *et al*. Hyaluronic acid-based nanoplatforms for Doxorubicin: A review of stimuli-responsive carriers, co-delivery, and resistance suppression. *Carbohydr. Polym*. **2021**, *272*, 118491, https://doi.org/10.1016/j.carbpol.2021.118491.
5. Martinho, N.; Santos, T.C.; Florindo, H.F.; Silva, L.C. Cisplatin-membrane interactions and their influence on platinum complexes activity and toxicity. *Front. Physiol*. **2019**, *9*, 1898, https://doi.org/10.3389%2Ffphys.2018.01898.
6. Parveen, A.; Ansari, M.A. Cisplatin, An Anticancer Drug: Clinical Uses and Side Effects. *Anusandhaan-Vigyaan Shodh Patrika* **2020**, *8*, 72-80.
7. Aldossary, S.A. Review on the pharmacology of cisplatin: clinical use, toxicity and mechanism of resistance of cisplatin. *Biomed. Pharmacol. J*. **2019**, *12*, 7-15, https://dx.doi.org/10.13005/bpj/1608.
8. Sobczak, M. A brief dive into the phenomenon of cisplatin resistance in non-small-cell lung cancer. *Acta Universitatis Lodziensis, Folia Bio et Oecologica* **2021**, *17*, 37-41, https://doi.org/10.18778/1730-2366.16.12.
9. Song, X.; Hu, Y.; Li, Y.; Shao, R.; Liu, F.; Liu, Y. Overview of current targeted therapy in gallbladder cancer. *Signal Transduct Target Ther*. **2020**, *5*, 230, https://doi.org/10.1038/s41392-020-00324-2.
10. Effendy, W.N.; Mydin, R.B.; Gazzali, A.M.; Sreekantan, S. Localised delivery of cisplatin from chitosan-coated titania nanotube array nanosystems targeting nasopharyngeal carcinoma. *Adv Pharm Bull* **2022**, in press, https://doi.org/10.34172/apb.2023.011.
11. Effendy, W.N.; Mydin, R.B.; Sreekantan, S.; Sopian, S.F.; Sundaraju, P.; Gunasagaran, S.; Gazzali, A.M. Titania Nanotube Arrays Nanosystem for Therapeutic Delivery of Resveratrol on Neuronal Cell lines Model. *Malaysian J. Med. Health Sci*. **2021**, *17*, 7 – 14.
12. Effendy, W.N.; Mydin, R.B.; Gazzali, A.M.; Sreekantan, S. Therapeutic nano-device: Study of biopolymer coating on titania nanotubes array loaded with chemodrug targeted for localized cancer therapy application. *IOP Conf. Ser.: Mater. Sci. Eng*. **2020**, *932*, 012116.
13. Shirazi-Fard, S.; Mohammadpour, F.; Zolghadr, A.R.; Klein, A. Encapsulation and Release of Doxorubicin from TiO_2 Nanotubes: Experiment, Density Functional Theory Calculations, and Molecular Dynamics Simulation. *J. Phys. Chem. B* **2021**, *125*, 5549-58, https://doi.org/10.1021/acs.jpcb.1c02648.
14. Hamedi, S.; Koosha, M. Designing a pH-responsive drug delivery system for the release of black-carrot anthocyanins loaded in halloysite nanotubes for cancer treatment. *Appl. Clay Sci*. **2020**, *197*, 105770, https://doi.org/10.1016/j.clay.2020.105770.

15. Zakeri, N.; Rezaie, H.R.; Javadpour, J.; Kharaziha, M. Effect of pH on cisplatin encapsulated zeolite nanoparticles: Release mechanism and cytotoxicity. *Mater. Chem. Phys*. **2021**, *273*, 124964, https://doi.org/10.1016/j.matchemphys.2021.124964.
16. Basotra, M.; Singh, S.K.; Gulati, M. Development and validation of a simple and sensitive spectrometric method for estimation of cisplatin hydrochloride in tablet dosage forms: application to dissolution studies. *Int. Sch. Res. Notices* **2013**, *2013*, https://doi.org/10.1155/2013/936254.
17. Fisher, J. *In vitro binding kinetics of hemofilter with cisplatin* (Doctoral dissertation UCSF, USA) **2016**.
18. Patil, G.P.; Rondiya, S.R.; Bagal, V.S.; Shivhare, S.; Cross, R.W.; Dzade, N.Y.; Jadkar, S.R.; Chavan, P. Field emission characteristics of double walled TiO_2 nanotubes. *ES Mater. Manuf*. **2021**, *13*, 76-81, https://dx.doi.org/10.30919/esmm5f1143.
19. Kunrath, M.F.; Vargas, A.L.; Sesterheim, P.; Teixeira, E.R.; Hubler, R. Extension of hydrophilicity stability by reactive plasma treatment and wet storage on TiO_2 nanotube surfaces for biomedical implant applications. *J. R. Soc. Interface* **2020**, *17*, 20200650, https://doi.org/10.1098/rsif.2020.0650.
20. Duarte, C.A.; Goulart, L.R.; Filice, L.D. *et al*. characterization of crystalline phase of TiO_2 nanocrystals, cytotoxicity and cell internalization analysis on human adipose tissue-derived mesenchymal stem cells. *Mater*ials **2020**, *13*, 4071, https://doi.org/10.3390/ma13184071.
21. Voltrova, B,; Hybasek, V,; Blahnova, V. *et al*. Different diameters of titanium dioxide nanotubes modulate SaOs-2 osteoblast-like cell adhesion and osteogenic differentiation and nanomechanical properties of the surface. *RSC Adv*. **2019**, *9*, 11341-55, https://doi.org/10.1039/C9RA00761J.
22. Benčina, M.; Iglič, A.; Mozetič, M.; Junkar, I. Crystallized TiO_2 nanosurfaces in biomedical applications. *Nanomaterials* **2020**, *10*, 1121, https://doi.org/10.3390/nano10061121.
23. Keeley, M.; Kisslinger, K.; Adamson, C.; Furlan, P.Y. Magnetically Recoverable and Reusable Titanium Dioxide Nanocomposite for Water Disinfection. *J. Mar. Sci. Eng*. **2021**, *9*, 943, https://doi.org/10.3390/jmse9090943.
24. Hazan, R.; Sreekantan, S.; Mat, I. Crystal structure of TiO_2 nanotube arrays anodized at different voltage for cell-metal interaction. *Mater. Sci. Forum* **2017**, *888*, 262-266, https://doi.org/10.4028/www.scientific.net/MSF.888.262.
25. Cotrut, C.M.; Ionescu, I.C.; Ungureanu, E.; Berbecaru, A.; Zamfir, R.I.; Vladescu, A.; Vranceanu, D.M. Evaluation of surface modification techniques on the ability of apatite formation and corrosion behavior in synthetic body fluid: An in vitro study. *Surf. Interfaces* **2021**, *22*, 100866. https://doi.org/10.1016/j.surfin.2020.100866.
26. Schramm, G. Pharmacopeia of the People's Republic of China. *Pharm Zentralhalle Dtschl*. **1955**, *94*, 173-5.
27. Husain, T.; Shoaib, M.H.; Ahmed, F.R.; Yousuf, R.I.; Farooqi, S.; Siddiqui, F.; Imtiaz, M.S.; Maboos, M.; Jabeen, S. Investigating Halloysite Nanotubes as a Potential Platform for Oral Modified Delivery of Different BCS Class Drugs: Characterization, Optimization, and Evaluation of Drug Release Kinetics. *Int J Nanomed*. **2021**, *16*, 1725-41, https://doi.org/10.2147/ijn.s299261.
28. Ouyang, C.; Zhang, S.; Xue, C.; Yu, X.; Xu, H.; Wang, Z.; Lu, Y.; Wu, Z.S. Precision-guided missile-like DNA nanostructure containing warhead and guidance control for aptamer-based targeted drug delivery into cancer cells in vitro and in vivo. *J. Am. Chem. Soc*. **2020**, *142*, 1265-77, https://doi.org/10.1021/jacs.9b09782.
29. Liu, Y.; Xie, C.; Zhang, F.; Xiao, X. pH-responsive TiO_2 nanotube drug delivery system based on iron coordination. *J. Nanomater*. **2019**, *2019*, https://doi.org/10.1155/2019/6395760.
30. Xu, J.; Zhou, X.; Gao, Z.; Song, Y.Y.; Schmuki, P. Visible-light-triggered drug release from TiO_2 nanotube arrays: a controllable antibacterial platform. *Angew. Chem*. **2016**, *128*, 603-7, https://doi.org/10.1002/ange.201508710.
31. Wong, R.S.; Dodou, K. Effect of drug loading method and drug physicochemical properties on the material and drug release properties of poly (ethylene oxide) hydrogels for transdermal delivery. *Polymers* **2017**, *9*, 286, https://doi.org/10.3390/polym9070286.
32. Al Zomor, A.K.; Alakhali, K.M. Stability of reconstituted Cefuroxime Axetil at different temperature storage conditions. *Pharmacie Globale* **2013**, *4*, 1-5.
33. Shaaban, S.; Shabana, S.M.; Al-Faiyz, Y.S.; Manolikakes, G.; El-Senduny, F.F. Enhancing the chemosensitivity of HepG2 cells towards cisplatin by organoselenium pseudopeptides. *Bioorg. Chem*. **2021**, *109*, 104713, https://doi.org/10.1016/j.bioorg.2021.104713.
34. Huang, J.Y.; Lai, Y.K. TiO_2-Based Surfaces with Special Wettability–From Nature to Biomimetic Application. In: *Wetting and Wettability*, Aliofkhazraei, M. (Ed.), IntechOpen **2015**, https://doi.org/10.5772/60826.

35. Montgomerie, Z.; Popat, K.C. Improved hemocompatibility and reduced bacterial adhesion on superhydrophobic titania nanoflower surfaces. *Mater. Sci. Eng.: C* **2021**, *119*, 111503, https://doi.org/10.1016/j.msec.2020.111503.
36. Escada, A.L.; Nakazato, R.Z.; Claro, A.P. Influence of anodization parameters in the TiO_2 nanotubes formation on Ti-7.5 Mo alloy surface for biomedical application. *Mater. Res*. **2017**, *20*, 1282-90, http://dx.doi.org/10.1590/1980-5373-mr-2016-0520.
37. Huang, L.; Chen, J.; Li, X.; Liu, H.; Li, J.; Ren, T.; Yang, Y.; Zhong, S. Polymethacrylic acid encapsulated TiO_2 nanotubes for sustained drug release and enhanced antibacterial activities. *New J. Chem*. **2019**, *43*, 1827-37, https://doi.org/10.1039/C8NJ04568B.
38. Wang, T.; Weng, Z.; Liu, X.; Yeung, K.W.; Pan, H.; Wu, S. Controlled release and biocompatibility of polymer/titania nanotube array system on titanium implants. *Bioact. Mater*. **2017**, *2*, 44-50, https://doi.org/10.1016/j.bioactmat.2017.02.001.
39. Aw, M.S.; Kurian, M.; Losic, D. Non-eroding drug-releasing implants with ordered nanoporous and nanotubular structures: concepts for controlling drug release. *Biomater. Sci*. **2014**, *2*, 10-34, https://doi.org/10.1039/C3BM60196J.
40. Jafari, S.; Mahyad, B.; Hashemzadeh, H.; Janfaza, S.; Gholikhani, T.; Tayebi, L. Biomedical applications of TiO_2 nanostructures: Recent advances. *Int J Nanomedicine* **2020**, *15*, 3447, https://doi.org/10.2147/ijn.s249441.
41. Park, J.; Cimpean, A.; Tesler, A.B.; Mazare, A. Anodic TiO_2 Nanotubes: Tailoring Osteoinduction via Drug Delivery. *Nanomaterials* **2021**, *11*, 2359, https://doi.org/10.3390/nano11092359.